# Local dynamics coupled to hydration water determines DNA-sequence-dependent deformability

H. Nakagawa,[1] Y. Yonetani,[2] K. Nakajima,[3] S. Ohira-Kawamura,[3] T. Kikuchi,[3] Y. Inamura,[3] M. Kataoka,[1,4,*] and H. Kono[2,†]

[1]*Neutron Biophysics, Quantum Beam Science Center, Japan Atomic Energy Agency, Tokai, Ibaraki 319-1195, Japan*

[2]*Molecular Modeling and Simulation, Quantum Beam Science Center, Japan Atomic Energy Agency, Kizugawa, Kyoto 619-0215, Japan*

[3]*J-PARC Center, Japan Atomic Energy Agency, Tokai, Ibaraki 319-1195, Japan*

[4]*Graduate School of Materials Science, Nara Institute of Science and Technology, 8916-5 Takayama, Ikoma, Nara 630-0192, Japan*

(Received 5 July 2013; published 29 August 2014)

Molecular dynamics (MD) simulations and quasielastic neutron scattering (QENS) experiments were conducted on two hydrated DNA dodecamers with distinct deformability: 5′CGCGAATTCGCG3′ and 5′CGCGTTAACGCG3′. The former is known to be rigid and the latter to be flexible. The mean-square displacements of DNA dodecamers exhibit so-called dynamical transition around 200–240 K for both sequences. To investigate the DNA-sequence-dependent dynamics, the dynamics of DNA and hydration water above the transition temperature were examined using both MD simulations and QENS experiments. The fluctuation amplitude of the AATT central tetramer is smaller, and its relaxation time is longer, than that observed in TTAA, suggesting that the AT step is kinetically more stable than TA. The sequence-dependent local base pair step dynamics correlates with the kinetics of breaking the hydrogen bond between DNA and hydration water. The sequence-dependent DNA base pair step fluctuations appear above the dynamical transition temperature. Together with these results, we conclude that DNA deformability is related to the local dynamics of the base pair steps, themselves coupled to hydration water in the minor groove.

DOI: 10.1103/PhysRevE.90.022723 PACS number(s): 87.15.H−, 78.70.Nx, 87.10.Tf

## I. INTRODUCTION

Amino acid sequences are encoded in base sequences of DNA. Noncoding genomic DNA regions are known to regulate gene expression through DNA-protein interactions. DNA-binding proteins contain motifs that enable them to recognize specific base sequences [1]. Therefore, biological function is governed not merely by the genetic code (the one-dimensional string of DNA bases) but also by the mechanical properties of DNA.

Double stranded DNA conformations and their hydration were studied by x-ray crystal structural analyses [2–4] and NMR spectroscopy [5]. Drew and Dickerson reported a detailed structure of hydration on a B-DNA dodecamer [2]. They found an extensive and regular hydration pattern in the minor groove of AATT at the central position where water molecules form bridges between purine N3 and pyrimidine O2 atoms in adjacent base pairs. They also reported that AT steps bent slightly towards the minor groove while TA steps bent towards the major groove, resulting in making the minor groove wider [4]. On the basis of such observation, they inferred that stable hydration is one of the factors responsible for the stability of B-DNA conformation. McAteer *et al.* showed, using NMR, that the large amplitude, slow conformational dynamics and distinct structural features are characteristic of TA steps irrespective of sequence context [5].

Structural analysis of dimer steps of DNA in protein-DNA complexes showed that the deformability of double helical DNA highly depends on its base sequence and the TA step was the most deformable of all dimeric steps [1]. Recently, structural bioinformatics analysis using a much larger number of protein-DNA complexes also indicated that minor grove narrowing is often associated with AT-rich sequences and the narrowed minor groove produces a strong electrostatic interaction with a positively charged residue of Arg; thereby proteins recognize the variations in DNA conformation [6]. Molecular dynamics (MD) simulations and crystal structures have revealed that pyrimidine-purine (YR) steps are flexible and purine-purine (RR) steps are of intermediate deformability, while purine-pyrimidine (RY) steps are stiff [7,8]. The most rigid and flexible steps are AT and TA, respectively [1,8]. The deformability of DNA upon protein binding is proportional to the extent of the thermal fluctuation of the DNA conformations [8]. Such a local fluctuation at the base pair level plays an important role in protein-DNA interactions. It is responsible for interbase hydrogen-bond breakage and the opening and closing of the structure at nucleotide pairs. Local DNA denaturation (the separation of the DNA double helix strands at specific sites) is a well-documented obligatory step for transcription initiation, because the base pair fluctuations allow and control the accessibility of the structure to host molecules, such as nucleases and polymerases.

MD studies before around 1995 poorly reproduced DNA conformations because of the difficulty in treatment of long-range electrostatic forces. Since the force field parameters for DNA and the treatment of electrostatic interaction which is important for highly charged molecules have been remarkably improved, MD simulation can produce stable trajectories comparable with crystallographic and NMR data [9,10]. Recent systematic MD studies on DNA sequences have found a correlation between the extent of DNA deformability and hydration in the DNA minor groove [11,12]. The hydration structure in the minor groove is classified by the base pair DNA deformability at its hydration site. The hydrogen-bond pattern of rigid base pair steps tends to be ordered, with one or two water molecules forming a hydrogen-bonded bridge between

*kataoka@ms.naist.ac.jp
†kono.hidetoshi@jaea.go.jp

 

the bases of distinct strands. On the other hand, flexible steps form no stable hydration water bridges. Furthermore, water-bridge kinetics is correlated with structural fluctuations of DNA [13]. These studies have elucidated the tightly coupled dynamics between DNA and its bound water molecules via hydrogen bonding.

The dynamical transition phenomenon of biomolecules, in which the amplitude of molecular fluctuation abruptly increases around 200–240 K, is induced by hydration [14,15]. This dynamical transition is connected to hydration structure and dynamics [16] through the glass transition of the hydration water [17]. The interactions between biomolecules and water have been elucidated within the past two decades [17–19]. In proteins, the dynamical transition is related to protein functionality, although the biological implication of this phenomenon is not fully understood [20]. At cryogenic temperatures, biomolecules fluctuate in a harmonic manner, and the glassy state is revealed in their boson peaks [21]. Dynamical transition and boson peaks have also been observed in DNA [21–23]. However, the relevance of DNA dynamical transition to biological phenomena has not been discussed to date. The putative origin of the glass transition is hydrogen-bond dissolution of bound water molecules on the DNA surface [24]. Therefore, the structural dynamics of DNA appear to rely critically on the dynamics of the hydration water. Furthermore, the dynamical transition of fibrous DNA occurs around 200–240 K, the transition temperature of hydration water [25]. The dynamical properties of DNA hydration water, particularly in the minor and major grooves, are quite different from those of bulk water. Interestingly, water molecules in the minor grooves are more structured than those residing in major grooves. Since DNA fibers are heterogeneous, i.e., comprise random mixtures of DNA bases A, T, G, and C, such measurements cannot clarify whether DNA dynamical transitions depend on nucleic acid sequence. Further experimental measurements using DNA of well-defined base sequence is required to reveal the relationship between the dynamical transition of DNA, the dynamics of hydration water, and sequence-dependent deformability.

The dynamical transition of biomolecules and its relevance to hydration has been extensively examined by incoherent quasielastic neutron scattering (QENS), which is a kind of inelastic neutron scattering [19]. QENS characterizes the atomic dynamics in both space and time [26], enabling quantitative comparisons between QENS data and MD simulation results [27]. Especially, QENS is suitable for examining the relaxation and/or diffusive dynamics of biomolecules. However, neutron scattering is unsuitable for investigating site specific local motion, because the incoherent QENS signal is averaged over all hydrogen atoms in the system. On the other hand, the dynamical information provided by MD simulation, which tracks the trajectories of individual atoms, is partitioned into contributions from the different constituents [28].

Here, to elucidate the sequence-dependent dynamical transition of DNA and the relationship between DNA and hydration water dynamics, we combined QENS experimental data with MD simulations of two DNA sequences, 5′CGCGAATTCGCG3′ and 5′CGCGTTAACGCG3′ (the central four sequences are highlighted by underlines). The former is known to be rigid and the latter to be flexible, as previously reported by MD study [8]. Our QENS experiments revealed the dynamical transitions in both sequences, suggesting that the dynamical transition is independent of DNA base sequence. Molecular fluctuation differences appear in the central tetramer regions, AATT and TTAA, at temperatures above the dynamical transition temperature, indicating a relationship between DNA deformability and anharmonic fluctuations. The sequence-dependent deformability arises from the local relaxation dynamics of the DNA base pair step, and is connected to the dynamics of hydration water.

## II. MATERIALS AND METHODS

### A. Quasielastic neturon scattering (QENS)

#### *1. Sample preparation*

Dodecameric DNA (sequences 5′CGCGAATTCGCG3′ and 5′CGCGTTAACGCG3′) were purchased from Sigma-Aldrich Japan. The DNA samples were used without further purification. The lyophilized DNA was dissolved in $D_2O$ to facilitate the exchange of all labile protons, and lyophilized. This procedure was repeated three times to ensure the complete proton exchange. The lyophilized samples were hydrated by equilibrating with KCl-saturated $D_2O$ solution. The hydration levels (g $D_2O$/g DNA) of AATT and TTAA sequences were 0.90 and 0.82, respectively. In DNA, exchangeable hydrogen atoms reside in the NH and $NH_2$ groups of the four nucleic acid bases and in phosphate groups. In DNA and $D_2O$ atomic species, the incoherent cross section of hydrogen atoms (about 80 b) largely dominates the coherent part (about 2 b), and also the coherent and incoherent cross sections of all other atoms (N, O, P, C, and D). The scattering contribution of DNA hydrated with $D_2O$ should mainly comprise incoherent scattering of nonexchangeable DNA hydrogen atoms.

#### *2. Data collection*

A time-of-flight technique was adopted for the QENS measurements, using the cold-neutron disk-chopper spectrometer AMATERAS installed in Materials and Life Science Experimental Facility (MLF) at the Japan Proton Accelerator Research Complex (J-PARC) [29]. In the experiment, three incident energies, 1.050, 1.685, and 3.132 meV, were used. For analysis, the data measured with the incident energy of 3.132 meV, which gave the highest intensity, was used. The energy resolution for this incident energy was determined by measuring the scattering from a vanadium specimen with the same shape as the sample. The full width of the elastic peak was $\sim$28 $\mu$eV, corresponding to observable motions beyond 148 ps. The observable length of the scattering vector $Q$ at the elastic position ranged from 0.5 to 2.0 Å$^{-1}$. To enable analysis of QENS, neutron scattering measurements were conducted at 100, 160, 200, 260, and 280 K for about 1 h, and at 300 K for 5–8 h. Each of the samples was stuffed in a hollow aluminum container of 10.0 mm external radius. The height of the sample holder was 30 mm. No multiple scattering corrections were required, because the sample transmission value was relatively large (about 90% of the total measurements). All obtained data were analyzed using the software suite UTSUSEMI [30]. The neutron differential scattering cross section is $d^2\sigma/d\Omega dE_f \propto (k_f/k_i)S(Q,E)$,

where $k_i$ and $k_f$ are amplitudes of the incident and final neutron wave vectors, respectively, $S(Q,E)$ is the dynamic structure factor, and $Q$ and $E$ are respective momentum and energy transfers. To obtain $S(Q,E)$, the data were divided by the solid angles of their detector pixels and by $k_f/k_i$. The neutron fluxes between data were normalized by the counts of the proton beam projected onto the neutron target.

#### 3. Data analysis of QENS

The hydrogen atoms whose dynamics are within the energy resolution are regarded as static and induce a strong elastic intensity [31]. In contrast, mobile hydrogen atoms with higher energy than the energy resolution yield QENS. This contribution, normally described as the Lorentzian distribution, is characterized by the half width at half maximum (HWHM or $\Gamma$ in equations). The dynamic structure factor $S(Q,\omega)$ can be written as the sum of a delta function and the Lorentzian terms, as follows:

$$S(Q,\omega) = \exp(-Q^2\langle u^2\rangle/3)\,[S_{\mathrm{EISF}}\delta(\omega) + (1-S_{\mathrm{EISF}})\,L(\Gamma,\omega)] \otimes R(\omega) + B_{\mathrm{BG}}, \quad (1)$$

where $R(\omega)$ is the resolution function, $\otimes$ denotes the convolution, and $\exp(-Q^2\langle u^2\rangle/3)$ is the Debye-Waller factor. The first term describes the elastic contribution, $\delta(\omega)$ is weighted by the elastic incoherent structural factor ($S_{\mathrm{EISF}}$), and the second term is the Lorentzian.

$$L(\Gamma,\omega) = \frac{1}{\pi}\frac{\Gamma(Q)}{\Gamma^2(Q)+\omega^2}. \quad (2)$$

$B_{\mathrm{BG}}$ means background scattering, and comes from vibrational motions. This contribution is regarded as being flat in the analysis.

### B. MD simulation

#### 1. System setup and simulation

MD simulations were performed on B-form DNA fragments 5′CGCGAATTCGCG3′ and 5′CGCGTTAACGCG3′. Water molecules were placed around each DNA fragment so as to cover the space of at least ∼8 Å from the DNA surface, on which a periodic boundary box with truncated octahedral shape was imposed. The numbers of water molecules were 5117 and 5111 for the AATT and TTAA systems, respectively. The DNA and water molecules were modeled by the force field parameters, amber *ff*99 [32,33] and TIP3P [34], respectively. To ensure electric neutrality and physiological ionic concentration (∼0.15$M$), 39 $K^+$ and 17 $Cl^-$ were added to the simulation box. Using the Sander module of AMBER8 [35], energy minimization was carried out at first, and MD simulations were performed. Atom configurations were equilibrated during the initial 2 ns, where DNA atom positions were restrained with harmonic potentials, but they were gradually released. In this equilibrium stage, pressure was kept at 1 atm and temperature was gradually changed to the target temperature (namely, 225, 250, 275, 300, and 325 K). After this equilibration, MD simulation was performed for 8 ns at each temperature. MD simulations were also carried out at lower temperatures (below 225 K), but here we do not discuss the results because of the statistical uncertainties arising from the slow relaxations at lower temperatures. Temperature and pressure were controlled by the weak coupling method [36]. Atom trajectories were generated by numerically integrating the equations of motion for each atom, while applying the SHAKE (bond geometry) constraints [37] to the covalent bonds involving hydrogen atoms. Long-range electrostatic interactions were calculated with the particle mesh Ewald method [38].

#### 2. Analysis of simulation data

The dynamic structure factor $S(Q,\omega)$ was calculated from the Fourier transformation,

$$S(Q,\omega) = \frac{1}{2\pi}\int I_{\mathrm{self}}(Q,t)\,e^{-i\omega t}dt, \quad (3)$$

where $I_{\mathrm{self}}(Q,t)$ is the self part of the intermediate scattering function,

$$I_{\mathrm{self}}(Q,t) = \langle e^{i\boldsymbol{Q}\cdot\boldsymbol{r}_j(t)}e^{-i\boldsymbol{Q}\cdot\boldsymbol{r}_j(0)}\rangle. \quad (4)$$

Here, $\boldsymbol{r}_j$ denotes the position of atom $j$; only hydrogen atoms were considered because hydrogen atoms dominate the intensity of neutron scattering. Ten scattering vectors $\boldsymbol{Q}$ were randomly generated on a unit sphere, and $I(Q,t)$ was obtained as the average of the contributions.

Atom mean-square displacements $\langle[\boldsymbol{r}_j(t)-\boldsymbol{r}_j(0)]^2\rangle$ were evaluated for DNA and hydration water, considering hydrogen atoms only.

Dynamics of hydration water can be characterized by hydrogen-bond lifetimes. The lifetime, $\tau_{\mathrm{HB}}$, of hydrogen bonds formed between DNA and water was calculated in a way typical of the time correlation function [39], $C(t) = \langle h(t)h(0)\rangle/\langle h(t)\rangle$. Here, $h(t)$ is 1 when a hydrogen bond of interest is formed, otherwise 0. Hydrogen-bond formation was judged using the criterion of less than 2.5 Å distance between the hydrogen atom and acceptor and less than 135° formed by the donor, hydrogen atom, and acceptor [40]. The lifetime $\tau_{\mathrm{HB}}$ was obtained as $\tau_{\mathrm{HB}} = \int_0^\infty C(t)dt$, which corresponds to the time when $C(t)$, under the assumption of exponential decay, decreases to $e^{-1}$.

## III. RESULTS

### A. Dynamic structure factor of DNA

The dynamic structure factor contains information on particle correlations and their time evolution. It is directly obtained from QENS measurements as a function of scattering vector $\boldsymbol{Q}$ and the energy transfer. Two-dimensional colored contour maps of the dynamic structure factor of 12-mer DNA (containing the AATT central tetramer) are shown in Fig. 1 where panels (a) and (b) are those obtained by QENS experiments at 100 and 300 K, and panel (c) is that obtained by MD simulation at 300 K. In the partially H/D exchanged DNA, the scattering mainly comes from the nonexchangeable hydrogen atoms that are mainly in the DNA backbone, the phosphate and sugar, and partially in the base, due to the H/D exchange at NH and $NH_2$ groups. At 100 K, a strong elastic peak appeared at $E = 0$ meV and little scatterings were observed in the inelastic region [Fig. 1(a)]. Thus, at cryogenic temperatures, the DNA experiences minimal thermal fluctuation. In contrast, at 300 K, quasielastic scatterings around the elastic peak were clearly observed [Fig. 1(b)], indicating the development of

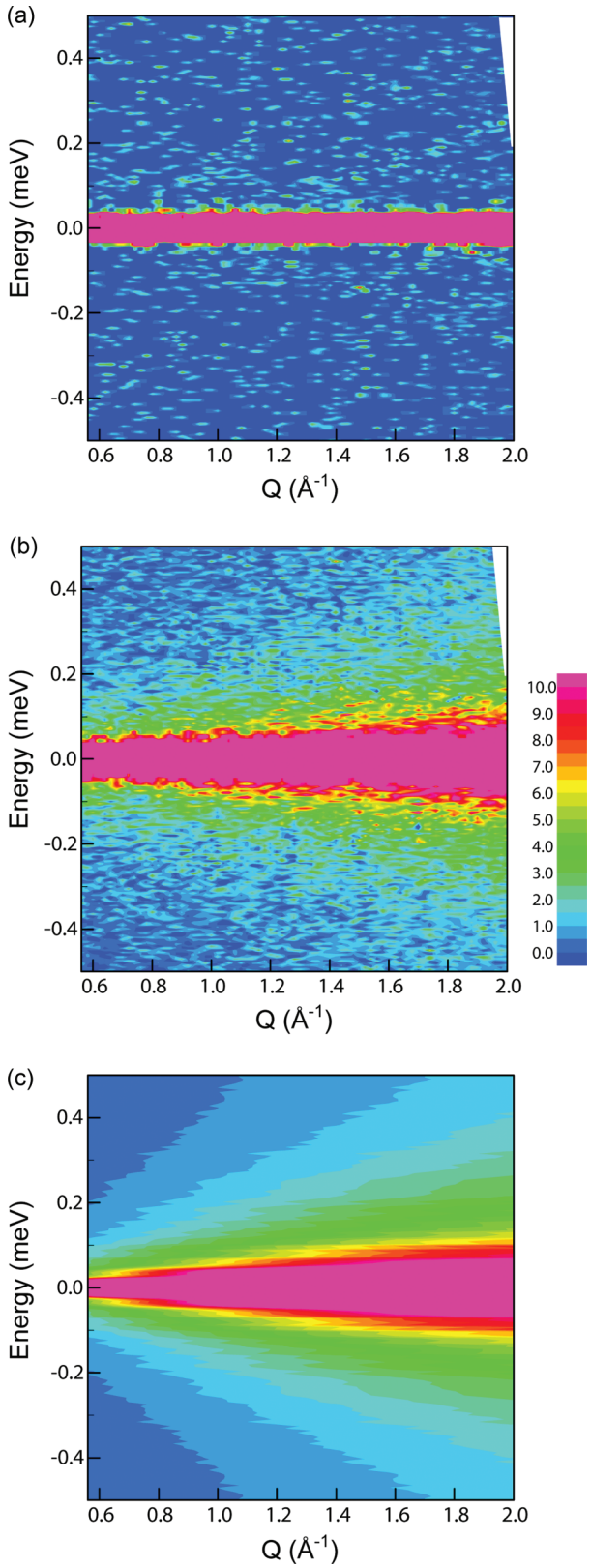


FIG. 1. (Color) Two-dimensional maps of dynamic structure factor of a dodecameric DNA sequence, 5′CGCGAATTCGCG3′. (a) Neutron scattering data at 100 K, (b) neutron scattering data at 300 K, (c) MD simulation at 300 K.

more rapid DNA motions than the instrumental time window of 148 ps. The QENS-measured dynamic structure factor of dodecamer DNA qualitatively agreed with that of the MD simulation [Fig. 1(c)], verifying the reliability of the $S(Q,E)$'s independently obtained from QENS experiments and MD simulations.

Actually, the differences in the experimental neutron spectra between AATT and TTAA are not so large. In the data analysis, the raw data have been carefully examined before the following data fitting analysis in order to judge if two spectra were different or not within the data noise. Figures 2(a) and 2(b) show the comparison of the elastic intensity and the inelastic intensity between the two sequences, respectively. To compare the data, the ratios $S(Q,\omega)_{\mathrm{TTAA}}/S(Q,\omega)_{\mathrm{AATT}} - 1$ were calculated. On the elastic intensity shown in Fig. 2(b), the ratios are distributed around zero in the $Q$ region, indicating that the data of the two sequences are essentially identical within the precision. On the contrary, the inelastic intensity shown in Fig. 2(b) exhibits significant deviations from zero. The deviation is symmetric, indicating that the origin of the difference between the two sequences is the intensity and/or width of the quasielastic scattering. The quasielastic scattering intensity of TTAA is approximately 20% larger than that of AATT at $\pm$ 0.4 meV. From these results, it can be concluded that the quasielastic scattering is more significant for TTAA than for AATT, indicating that TTAA is more flexible than AATT. This preliminary analysis convinced us to advance more quantitative analyses (see also Figs. 3 and 4).

### B. Dynamical transition of DNA

Dynamical transition was evaluated by the temperature-dependent mean-square displacement (MSD) [19,26]. Figure 3(a) shows the elastic incoherent scattering intensities of the DNA dodecamer containing the central AATT tetramer. The averaged MSD of the individual hydrogen atoms is obtained from the incoherent neutron scattering analysis assuming a Gaussian distribution [41];

$$S(Q,0) = A\exp(-\langle u^2\rangle Q^2/3), \tag{5}$$

where A and $\langle u^2\rangle$ are constants and the MSD is averaged over all hydrogen atoms. Figure 3(b) shows the MSD of both DNA sequences at various temperatures. Below 200 K, the MSD of both samples was suppressed, suggesting that DNA exists in the glassy state at these lower temperatures. At the higher temperature range, the MSDs increased with increasing temperature in both sequences. Dynamical transitions of both DNA sequences appeared around 200–240 K. The dynamical transition of heterogeneously sequenced DNA fibers occurs at a similar temperature [22]. These results suggest that the existence of the transition is independent of base pair step deformability. Above the transition temperature, the MSDs of both DNA sequences were not different within statistical error.

The experimentally obtained MSD values were averaged across the DNA dodecamer. To elucidate the MSD at the specific site of the central tetramer, we conducted MD simulations on these DNA sequences above the dynamical transition temperature. The MSDs of the central tetramer TTAA exceeded those of the AATT above the transition temperature [the main panel in Fig. 3(c)], in contrast to the behavior of the dodecamers for which the difference is not clear between the two sequences [inset in Fig. 3(c)]. The difference

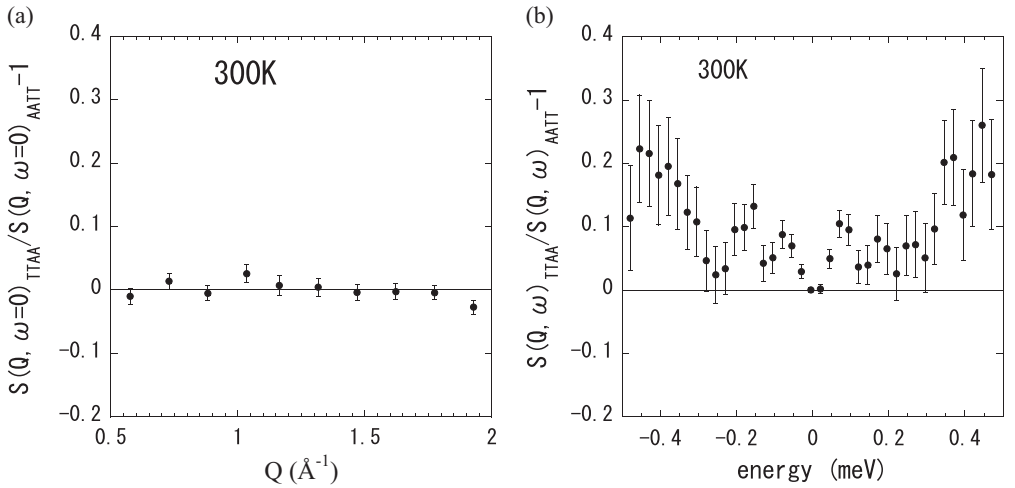


FIG. 2. (a) Comparison of elastic scattering intensities for two dodecameric DNA sequences, TTAA and AATT at 300 K. (b) Comparison of quasielastic scattering intensities for two dodecameric DNA sequences, AATT and TTAA at 300 K. In the plot, $S(Q,\omega)$ were calculated as a value where $S(Q,\omega)$ were accumulated for $Q$ between 0.5 and 2.0 Å$^{-1}$. $S(Q,\omega)$ for AATT and TTAA are scaled by the intensity at the elastic position before the calculation of the ratio.

in MSD between the two "dodecamer" DNAs was invisible because averaging MSDs over the entire 12-mers including the common 8-mers wiped out the sequence difference.

These results show that the dynamical transition is common to both sequences, and is independent of the DNA deformability. Interestingly, above the dynamical transition temperature, the central tetramer is subject to the deformability-dependent fluctuations.

### C. Curve fitting analysis of quasielastic scattering

To characterize the relaxation and/or diffusive dynamics and the geometry of structural DNA fluctuations at 300 K, we analyzed the quasielastic scattering. At 300 K, a quasielastic scattering intensity is dependent on $Q$; in the region of higher $Q$, the width of strong quasielastic scattering increased [Figs. 1(b) and 1(c)], which shows the contribution from mobile hydrogen atoms. Curve fitting by a single Lorentzian function as well as the double one showed that the scattering profile was adequately described by a single Lorentzian function [Eq. (1)] because the fit with the double Lorentzian was unstable and failed to converge. This indicates that the internal motion of DNA is represented as a single averaged mode. The fitted spectra of the quasielastic scattering from the DNA dodecamer containing the central AATT tetramer are shown in Fig. 4(a), demonstrating that the experimental data are reasonably fitted by a single Lorentzian model function.

### D. Amplitude of DNA dynamics

EISF data provide information on the conformational space geometries of DNA dynamics. The experimental $S_{\mathrm{EISF}}$ is plotted in Fig. 4(b). The $S_{\mathrm{EISF}}$ includes the contribution from both of the coherent and incoherent scatterings. However, according to our calculations using the MD data, the incoherent contribution is dominant, and the coherent one is negligible above 0.4 Å$^{-1}$. Therefore, the coherent scattering and anything other than incoherent one do not affect the EISF profiles (data not shown). Figure 4(b) shows that the $S_{\mathrm{EISF}}$ values of the AATT-containing dodecamer slightly exceed those of the TTAA-containing dodecamer in the lower $Q$ region. In the higher $Q$ region, the $S_{\mathrm{EISF}}$ values of both DNA sequences are similar. The geometry of DNA fluctuations can be described by fitting an analytical model to the EISF. The continuous diffusion model [42], diffusion within a spherical volume ($M_{\mathrm{DSV}}$), was found to not adequately fit the EISF, possibly because it did not fit the shoulder appearing around $Q$ = 1.0–1.5 Å. To provide a better fit, a two-side jump ($M_{\mathrm{2SJ}}$) diffusion model [31] was added to $M_{\mathrm{DSV}}$:

$$S_{\mathrm{EISF}} = p + (1-p)\, M_{\mathrm{DSV}} M_{\mathrm{2SJ}}. \tag{6}$$

The DSV model, which is parametrized by the radius of a hard-walled sphere $r$, is given as

$$M_{\mathrm{DSV}} = \left[\frac{3 j_1(Qr)}{Qr}\right]^2. \tag{7}$$

The 2SJ model is parametrized by the jump distance $R$ and is given by

$$M_{2SJ} = \tfrac{1}{2}\left[1 + j_0(2QR)\right]. \tag{8}$$

Here, $p$ and $(1-p)$ denote the fractions of immobile and mobile protons in the DNA, respectively, and $j_0(x)$ and $j_1(x)$ are the zero- and first-order Bessel functions, respectively. In this equation, $p$ accounts for the H atoms that do not undergo DSV motions or 2SJ motions on the measured time scale. Radii of spheres were determined as $r = 1.67 \pm 0.52$ Å and $r = 1.72 \pm 0.26$ Å for AATT and TTAA, respectively, with respective fractions of mobile protons $0.59 \pm 0.07$ and $0.59 \pm 0.04$. These results agree within experimental error. The conformational space (range of space accessible to the scatterers) of the proton diffusion of both sequences is similar. However, the jump distances of AATT and TTAA are statistically different: $R = 2.04 \pm 0.10$ Å for AATT and $R = 2.62 \pm 0.18$ Å for TTAA. This indicates that the differences in amplitude of dynamics are observed as the differences in the jump distance.

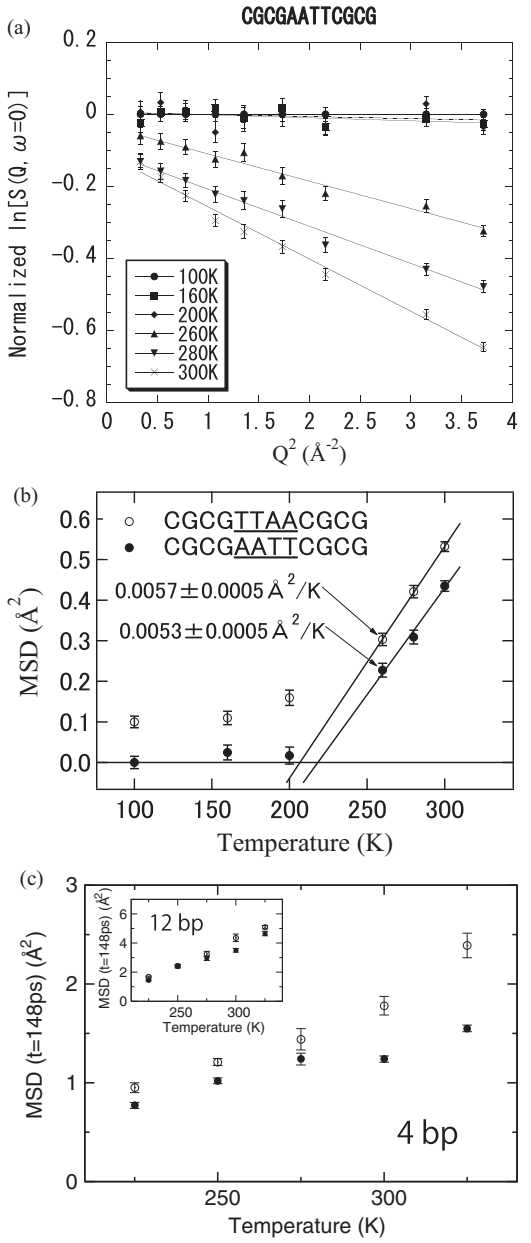


FIG. 3. (a) Elastically scattered neutron intensities of CGCGAATTCGCG sequence. The scattered intensities, corrected and normalized, are plotted as $\ln[S(Q, \omega = 0)]$ versus $Q^2$. The data are obtained at six temperatures. Solid lines are linear regressions on the data points; their slope gives the corresponding mean-square displacement. (b) Mean-square displacements of DNA sequences CGCGAATTCGCG and CGCGTTAACGCG, which were obtained from neutron scattering experiments. The linear fit was between 260 and 300 K. Data representing TTAA-containing dodecamers are shifted along the ordinate by 0.1 for the sake of clarity. (c) Mean-square displacements of DNA estimated from MD simulations at 225, 250, 275, 300, and 325 K: results for the central four base pairs, AATT and TTAA (main panel), and for the DNA dodecamer (inset).

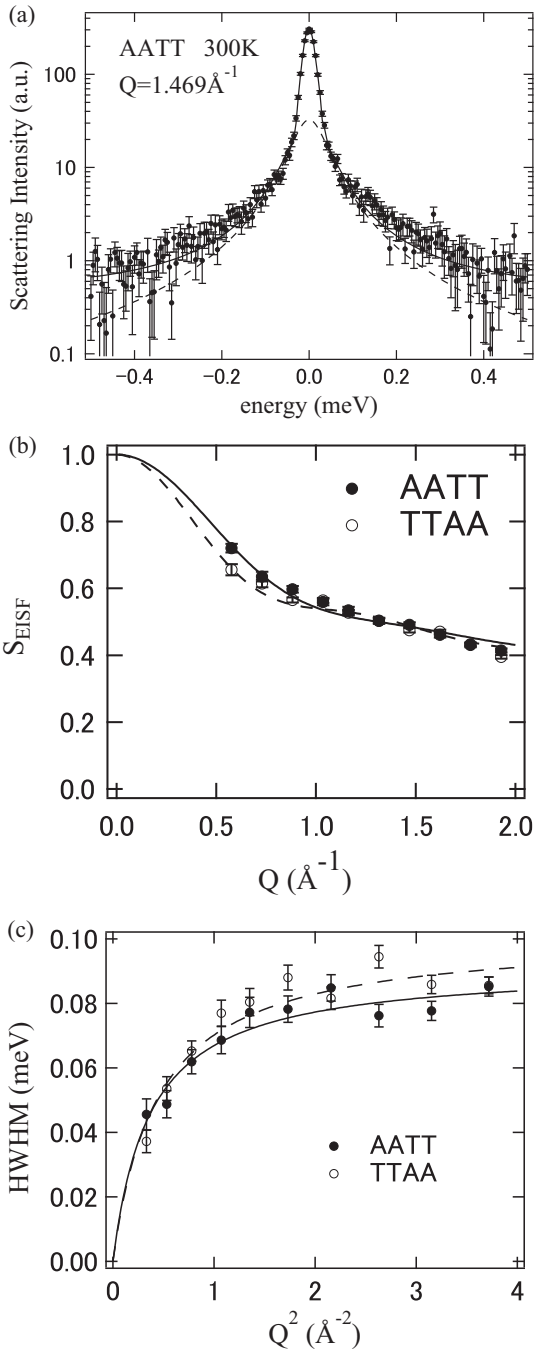


FIG. 4. (a) Quasielastic neutron scattering spectra of CGCGAATTCGCG sequence at $Q = 1.469$ Å$^{-1}$ and 300 K. Solid and dashed curves indicate a fitting curve by Eq. (1) and its Lorentzian component, respectively. (b) EISF for both sequences. Lines are fitting curves by Eq. (9). (c) HWHM as a function of $Q^2$ fitted with a jump diffusion model for both sequences. The values at $Q = 3.72$ Å$^{-1}$ almost coincide with each other.

### E. Relaxation time of DNA dynamics

Examining the HWHM as a function of $Q$ provides insight into the length-scale dependence of the corresponding motion time scale. HWHM of the Lorentzian is plotted as a function of $Q^2$ in Fig. 4(c). This plot provides information on the relaxation time of the DNA dynamics. In the lower $Q$ region, the HWHM of both sequences increases with $Q^2$ and approaches an asymptote at large $Q$. The asymptote of the TTAA-containing dodecamer is higher than the AATT, although both dodecamers behave similarly in the low-$Q$

region. This indicates that both sequences have a similar frequency of diffusive motion at longer length scales whereas at shorter length scales, the frequency of TTAA motion exceeds that of AATT. The HWHM plateau in the high-$Q$ region indicates that the correlation times are independent of length scale, suggesting that the jump motion dominates at smaller length scales. The previous MD simulation indicated that the forming and breaking dynamics of the hydrogen bond between DNA and water is dependent on DNA sequence and the flexibility of DNA is highly correlated with this local two-state jump dynamics between the bonding and nonbonding states [11,13]. To see the $Q$-dependent HWHM ($\Gamma$), the jump diffusion model [31] was employed, which is defined as

$$\Gamma(Q) = \frac{DQ^2}{1 + DQ^2\tau_0}. \tag{9}$$

The fitted curves to the data are shown in Fig. 4(b) The diffusion coefficients $D$, $6.0 \pm 0.8$ and $5.5 \pm 0.5$ ($10^{-8} \times \mathrm{nm}^2 \times \mathrm{s}^{-1}$) for AATT and TTAA, respectively, are identical within statistical error. The residence time of a hydrogen atom on one site is calculated as $\tau = 1/\Gamma(Q \to \infty)$, where $\Gamma(Q \to \infty)$ is the observed asymptotic HWHM. We find that $\tau = 45.2 \pm 1.5$ ps and $\tau = 40.9 \pm 1.1$ ps for AATT and TTAA, respectively. These results are statistically different, and the residence time of AATT is longer than that of TTAA. The local jump motion is related to the local potential energy barrier imposed on a proton by its environment. The height of this potential barrier is related to the residence time by the Arrhenius equation [31],

$$\tau = \tau_0 \exp\left(\frac{E_a}{k_B T}\right), \tag{10}$$

where $E_a$ is the activation energy. Assuming the same preexponential factor $\tau_0$ for both sequences, the activation energy difference between the sequences, $\Delta E_a$, is $0.0596 \pm 0.0248$ kcal/mol.

We estimated here the contribution from the DSV. In the DSV model, HWHM is independent of $Q$ in the low-$Q$ range, and then the DSV contribution gives a nonzero value in HWHM as $Q$ approaches 0. Here, the data below 0.4 $\mathrm{Å}^{-1}$ were not used for analysis due to the limit of detection. The DSV contribution did not clearly appear in HWHM in the observed $Q$ range. However, the HWHMs for AATT and TTAA sequences tend toward similar values as $Q$ decreases. This suggests that the DNA molecules are undergoing constrained diffusive motions with similar correlation times. Therefore, the sequence-dependent DNA dynamics cannot be explained by the DSV model. The HWHM [Fig. 4(c)] shows similar $DQ^2$ dependency in the lower $Q$ range, but gives different values between the two sequences in the higher $Q$ range, which indicates that the jump motions essentially produce the sequence-dependent dynamics. This is consistent with the physical picture derived from the EISF analysis.

### F. Dynamical relation between DNA and hydration water

The dynamical relation between DNA and hydration water was explored by MD simulation analysis, where water molecules whose oxygen had a distance smaller than 3.5 Å from any DNA atom were regarded as hydration water (see graphical view in Fig. 5).

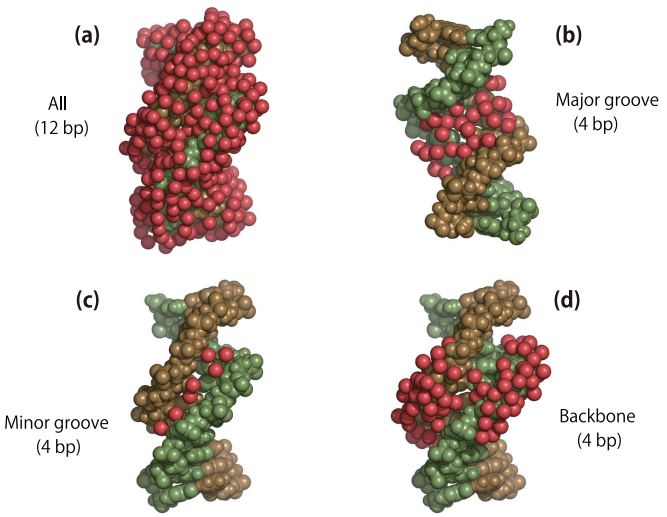


FIG. 5. (Color) Hydration water molecules in four different regions: (a) All 12 base pair DNA, and (b) major groove, (c) minor groove, and (d) phosphate backbone in the central four base pair region. Water molecules within 3.5 Å of DNA surface are shown by the oxygen sites (red). The DNA strands are depicted in green and yellow. Configurations of DNA and hydration water molecules were taken from the MD simulation of CGCGAATTCGCG at 300 K.

MSDs of the hydration water molecules are shown in Fig. 6(a). The MSDs show a similar tendency to those for DNA [Figs. 3(b) and 3(c)]; the values gradually increase as temperature increases. However, the discussion with the MSDs is not definite, particularly in the quantitative assessment, because the hydration water molecules frequently exchange with those in the outer region; MSD values $\langle[\boldsymbol{r}_j(t) - \boldsymbol{r}_j(0)]^2\rangle$ include all trajectories of water molecules that are regarded as hydration water at $t = 0$, thus, it still counts after the water departs from the hydration layer. Analysis of hydrogen-bond lifetime $\tau_{\mathrm{HB}}$ makes this point clear because $\tau_{\mathrm{HB}}$ includes events in the hydration layer only. Figure 6(b) shows the plot of $1/\tau_{\mathrm{HB}}$. We can observe a similar tendency as seen in MSDs [Fig. 6(a)]. Hydrogen-bond lifetime steeply increases and is over a few hundred picoseconds at 225 K. The current MD duration time was not long enough to obtain reliable statistics at such low temperatures and was difficult to discuss the dynamical transition of hydration water.

Between AATT and TTAA sequences, no remarkable difference is seen in any case of MSD [Fig. 6(a)] and $1/\tau_{\mathrm{HB}}$ [Fig. 6(b)] when we considered the hydration on the entire 12-mers. However, the detailed analysis on local, different regions of hydration, shown in Figs. 6(c) and 6(d), provided a further microscopic feature; the behaviors of hydration water in most cases provided essentially the same for the AATT and TTAA cases, but a remarkable difference appears in the minor grooves. That is, hydration water in the minor groove is sensitive to DNA sequence. It has been shown that the sequence dependence of hydration water appears exclusively in the minor groove [11]. Figure 6(d) shows hydrogen-bond lifetimes in the major and minor grooves, and in the vicinity of

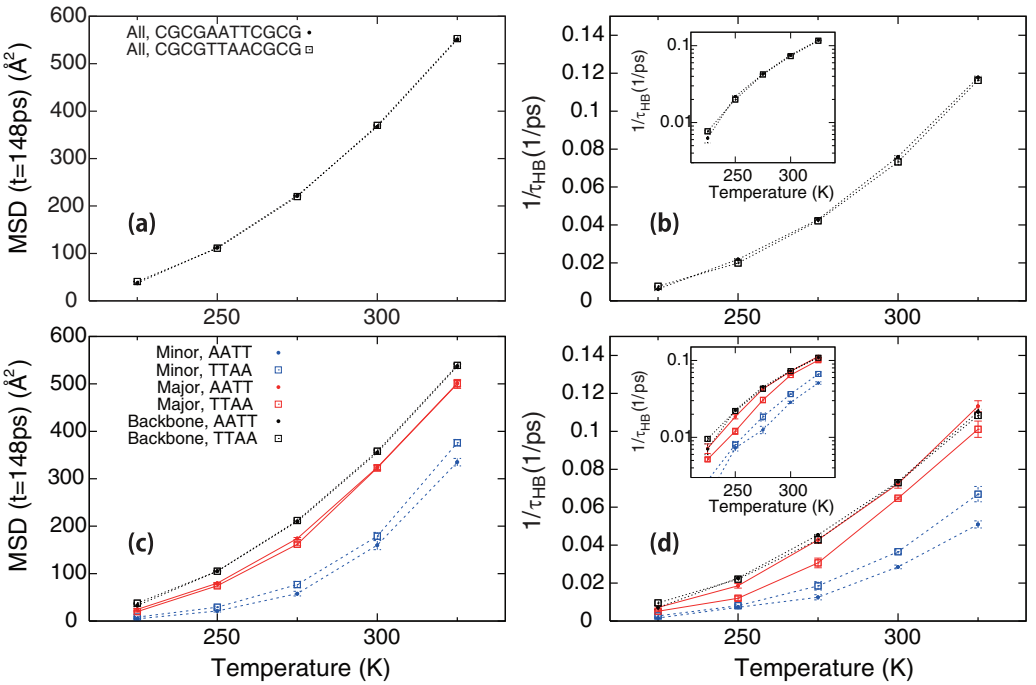


FIG. 6. (Color) Mean-square displacement of hydration water (a) and (c) and DNA-water hydrogen-bond lifetimes $\tau_{HB}$ (b) and (d), from MD simulations. Note that the ordinates in the insets of the (b) and (d) panels are in a logarithm scale. (a) and (b) are the results for entire regions and (c) and (d) for local regions shown in Fig. 5. Error bars are given in any panels (a)–(d), though they are too small to be seen in most cases.

the phosphate backbone. At lower temperatures, the lifetime is very long in any region (e.g., $\tau_{HB}>100$ ps at 225 K), but at about 300 K, it is significantly reduced (e.g., about $\tau_{HB}\sim15$ ps in the major groove and in the vicinity of the phosphate backbone). The minor groove still shows somewhat larger lifetimes, ~40 ps. The difference in lifetime reflects the difference of the surface geometry, as shown in previous MD studies [43,44]. In narrow and less exposed regions such as the DNA minor groove, water molecules are likely to reside for a long duration. Though surface geometry has been recognized as one of dominant factors for determining surface water properties, the origin of such different lifetimes has recently been interpreted in terms of hydrogen-bonding patterns [13] and excluded volume [45].

## IV. DISCUSSION

We have clarified the sequence-dependent and sequence-independent dynamical properties of DNA and its hydration water. We found that the dynamical transition of DNA occurs regardless of the deformability, and that the base pair step fluctuations appear above the dynamical transition temperature. This base pair step dependent fluctuation is coupled to the dynamics of water, particularly the difference between the sequences appears in the minor groove. The linking mechanism is hydrogen bonding between DNA and water molecules. We now discuss the dynamical transition, deformability of DNA, the local base pair step fluctuation and its relationship to sequence-dependent hydration water dynamics, compatibility between QENS and MD, and some problems inherent in the current MD.

### A. Dynamical transition of DNA

Local conformational changes, such as jumps of atoms from one configuration to another, and their collective motions, typically occur at terahertz-scale frequencies. The biomolecular dynamics in this frequency range shares many similarities with those of glass forming liquids. At low temperatures, the so-called boson peak, which is characteristic of glass spectra, arises in DNA [21] as well. Fast picosecond relaxation at an ambient temperature occurs similarly in the glass transition [21,22]. Increased biomolecular flexibility is a direct consequence of the glass transition of solvent, expressed as dynamical changes in the solvent environment [46]. The glass transition of hydration water is followed by an abrupt change in protein structural flexibility at about 170 K. These changes are detectable by the inelastic neutron scattering at the higher temperature, about 200 K [17].

Inelastic and quasielastic scattering experiments were performed on DNA fiber [21,22], while MD simulations were conducted on DNA strands of defined base sequence [23]. In this study, neutron scattering experiments and MD simulations were performed on two dodecameric DNA sequences of significantly different deformability, as already established by MD simulation [11–13]. Dynamical transitions in both DNA dodecamers were clearly demonstrated in the neutron experiment. It should be emphasized that this transition occurred independently of DNA sequences. Recently, the dynamical transition of proteins was found to occur independently of the species of the polypeptide chain [47] or protein conformation [48]. Similarly, DNA dynamical transition does not depend on specific base sequence. Therefore we conclude that, in general, dynamical transitions of biomolecules require

no specific structures or base compositions. The transition is a common dynamical property of hydrated biomacromolecules, and is coupled to the dynamics of hydration water.

### B. Interpretation of neutron data by MD simulation

The absolute values of the MSDs derived from the neutron experiment are approximately one order smaller than those derived from the MD simulation. One of the causes of this discrepancy is the difference of the aqueous environment between the hydrated powder DNA sample in the neutron experiment and the solution DNA in the MD simulation. In the MD system which mimics physiological solute conditions, there is the bulk water around the hydrated DNA. In the experimental powder sample, such bulk water does not exist. The different aqueous environments lead to the quantitative inconsistency in the obtained dynamical parameters. The MD simulations in solution and crystal (similar to powder) have demonstrated that the molecular-molecular interactions as well as the aqueous environment affect the absolute values of the dynamical parameters [27,49]. In the present system, it was also found that the diffusion and the relaxation dynamics as well as the MSDs of the hydrogen atoms in the DNA are systematically suppressed in the neutron experiment compared with those in the MD simulation. Another cause of the inconsistency is an approximation in the neutron data analysis where the Gaussian approximation widely used can underestimate the MSD [50]. Therefore, in the present paper, the absolute values of the dynamical parameters derived from the neutron experiment and the MD simulation are not discussed. In spite of the quantitative inconsistency, the previous works [22,23,25] as well as this study demonstrated that the DNA dynamical transition is observed. The dynamical values derived from the neutron experiment and the MD simulation exhibit the qualitative consistency; both give $D_{\mathrm{AATT}} \approx D_{\mathrm{TTAA}}$ and $\tau_{\mathrm{AATT}} > \tau_{\mathrm{TTAA}}$. This qualitative consistency should justify the dynamical picture suggested by the QENS analysis. The quantitative discrepancy between the neutron experiment and the MD simulation mainly comes from the difference of the aqueous environments. Because the environmental difference is thought to systematically affect the dynamics, the conclusion on the relationship between the dynamical transition and the deformability of DNA will still be valid.

DNA-sequence-dependent conformation is characterized by six conformational parameters (shift, slide, twist, rise, roll, and tilt) [1], which describe the local geometry of each base pair step. The internal DNA energy is often quantified by calculating the sum of harmonic functions along the conformational coordinates. The corresponding force parameters and equilibrium geometries are estimated from the observed distributions of these conformational variables in protein-DNA complexes [1]. However, thermal fluctuations of DNA base pair steps behave stochastically rather than harmonically at room temperature [13]; a DNA base pair step resides at a stable configuration for a while, but sometimes suddenly changes into another stable state (Fig. 6 in Ref. [13]). The MD trajectories suggest the TTAA base pair step has a larger jump than the AATT step. The same tendency was confirmed by the present quasielastic scattering analysis, which revealed that TTAA fluctuations occur in shorter relaxation times [see Fig. 4(b)] and have longer jump distances (that is, larger amplitude of DNA dynamics) [see Fig. 4(c)] compared with AATT fluctuations.

It should be noted that dynamical differences between the two DNA sequences cannot be observed clearly in MSD analysis of elastic scattering intensity. Rather, these differences can be detected by quasielastic scattering. This fact embodies the essential advantage of quasielastic scattering analysis over elastic scattering at a single energy resolution. Elastic scattering provides an averaged MSD across the whole system, while quasielastic scattering enables the analysis of both time and length dynamics.

### C. Dynamical transition and DNA deformability

Our present work provides two contrast results: (1) The dynamical transition of DNA occurs regardless of the deformability of DNA double helical structure, which is independent of DNA base sequence, and (2) DNA-sequence-dependent fluctuation appears above the dynamical transition temperature. As the previous works demonstrated, the two sequences of DNA have different mechanical properties in the physiological environment; AATT is rigid and TTAA is flexible [1,8]. The former result suggests that the appearance of the dynamical transition is not correlated with this mechanical property. Although this result might be trivial and boring, apparently, we would like to equivalently emphasize the sequence-independent and sequence-dependent properties. The present results show that the dynamical transition itself is a common physical property of DNA, and interestingly the sequence-dependent dynamics is hidden below the transition temperature, probably due to the vitrification of the DNA molecule. The combining of these two results more strongly indicates that the DNA-sequence-dependent dynamics is linked to the dynamical transition.

### D. Limitations in the current MD simulations and future prospects

#### *1. Molecular models and force field parameters*

The molecular structure and dynamics in MD are dependent on the parameters, such as the force field and water model. In the present work, TIP3P [34] was chosen as a water model, as the consequence of accounting the compatibility with the DNA parameters used. This combination is suitable for the simulation at 300 K and has been used in many studies. It is notable that various improvements have recently been made to force fields of DNA [51], water [52,53], and ions [54]. Although these updated force fields demand a more computational cost, a more reliable, quantitative evaluation may be possible in the future.

As a relevant topic, it is important to note an MD study by Biswal *et al.* [25], which reports quantitative evaluation of the dynamic transition temperature in DNA and the hydration water. They employed the five-site water model, TIP5P [52], which is especially tuned for the temperature dependence of water thermodynamics [52,55]. With the TIP5P model, they showed that the DNA hydration water exhibits dynamic transition at 255 K, which is a slightly higher temperature than that of the liquid-liquid transition in bulk water, 247 K [25]. It was also reported that the dynamical transition occurs with the TIP3P system, although the transition was not

as prominent [18]. In our work, it is not our purpose to determine the exact transition temperature for both DNA sequences by MD simulation. It is rather reasonable to use TIP3P in order to examine the dynamics of the DNA and the hydration water above the transition temperature and study their relationship with the deformability of the DNA at physiological temperature.

#### 2. *Quantum effect of light and heavy hydrogen atoms*

Another limitation inherent in the current MD simulation concerns the nuclear quantum effect for H and D atoms. The quantum effect in general becomes more dominant at low temperatures. The quantum effect has been confirmed in several cases of water [56] and hydrogen [57] using quantum MD simulation. In the present MD simulations, the force fields used are all based on the classical model and do not include nuclear quantum effects explicitly. We expect, however, that the current MD analysis can capture the essence of the DNA-sequence-dependent character. This is because sequence-dependent behavior of interest to us appears at ∼300 K. Another reason is that the hydrogen atoms considered here are covalently bonded to the DNA heavy atoms. In this case, the hydrogen motions are affected by the DNA conformational motion, and contribution from the quantum effect will be relatively small. Finally, we note that we focused the analysis on the difference in dynamics between AATT and TTAA. If the similar extents of quantum effects in both sequences are assumed, the difference will not change fundamentally. Yet, the nuclear quantum effect is indeed important, particularly when quantitatively characterizing low-temperature dynamics of water and hydrogen. A more explicit treatment for the effects will reveal how the nuclear quantum effect influences the low-temperature dynamics.

## ACKNOWLEDGMENTS

We thank the technical support team of J-PARC Center for their help in the experiment. This work was partly supported by grants-in-aid for scientific research from the Ministry of Education, Science, Sports, Culture, and Technology of Japan awarded to H.N. (Grants No. 22113521 and No. 23650469), Y.Y. (Grant No. 23740321), and H.K. (Grants No. 18031042 and No. 23114723). The QENS experiment was approved by the Neutron Science Proposal Review Committee of J-PARC/MLF (Proposal No. 2010A0042). H.N. and Y.Y. contributed equally to this work.

[1] W. K. Olson, A. A. Gorin, X.-J. Lu, L. M. Hock, and V. B. Zhurkin, Proc. Natl. Acad. Sci. USA **95**, 11163 (1998).
[2] H. R. Drew and R. E. Dickerson, J. Mol. Biol. **151**, 535 (1981).
[3] H. R. Drew, R. M. Wing, T. Takano, C. Broka, S. Tanaka, K. Itakura, and R. E. Dickerson, Proc. Natl. Acad. Sci. USA **78**, 2179 (1981).
[4] D. R. Mack, T. K. Chiu, and R. E. Dickerson, J. Mol. Biol. **312**, 1037 (2001).
[5] K. McAteer, P. D. Ellis, and M. A. Kennedy, Nucleic Acids Res. **23**, 3962 (1995).
[6] R. Rohs, S. M. West, A. Sosinsky, P. Liu, R. S. Mann, and B. Honig, Nature **461**, 1248 (2009).
[7] F. Lankaš, J. Šponer, J. Langowski, and T. E. Cheatham, III, Biophys. J. **85**, 2872 (2003).
[8] S. Fujii, H. Kono, S. Takenaka, N. Go, and A. Sarai, Nucleic Acids Res. **35**, 6063 (2007).
[9] S. Louise-May, P. Auffinger, and E. Westhof, Curr. Opin. Struct. Biol. **6**, 289 (1996).
[10] T. E. Cheatham, III, Curr. Opin. Struct. Biol. **14**, 360 (2004).
[11] Y. Yonetani and H. Kono, Biophys. J. **97**, 1138 (2009).
[12] Y. Yonetani, H. Kono, S. Fujii, A. Sarai, and N. Go, Mol. Simul. **33**, 103 (2007).
[13] Y. Yonetani and H. Kono, Biophys. Chem. **160**, 54 (2012).
[14] H. Nakagawa, Y. Joti, A. Kitao, and M. Kataoka, Biophys. J. **95**, 2916 (2008).
[15] J. H. Roh, V. N. Novikov, R. B. Gregory, J. E. Curtis, Z. Chowdhuri, and A. P. Sokolov, Phy. Rev. Lett. **95**, 038101 (2005).
[16] H. Nakagawa and M. Kataoka, J. Phys. Soc. Jpn. **79**, 083801 (2010).
[17] W. Doster, J. Non-Cryst. Solids **357**, 622 (2011).
[18] W. Doster, Biochim. Biophys. Acta **1804**, 3 (2010).
[19] W. Doster, S. Cusack, and W. Petry, Nature **337**, 754 (1989).
[20] B. F. Rasmussen, A. M. Stock, D. Ringe, and G. A. Petsko, Nature **357**, 423 (1992).
[21] A. P. Sokolov, H. Grimm, and R. Kahn, J. Chem. Phys. **110**, 7053 (1999).
[22] S.-H. Chen, L. Liu, X. Chu, Y. Zhang, E. Fratini, P. Baglioni, A. Faraone, and E. Mamontov, J. Chem. Phys. **125**, 171103 (2006).
[23] J. Norberg and L. Nilsson, Proc. Natl. Acad. Sci. USA **93**, 10173 (1996).
[24] J. Laudát and F. Laudát, Europhys. Lett. **20** 663 (1992).
[25] D. Biswal, B. Jana, S. Pal, and B. Bagchi, J. Phys. Chem. B **113**, 4394 (2009).
[26] G. Zaccai, Science **288**, 1604 (2000).
[27] M. Tarek and D. J. Tobias, Biophys. J. **79**, 3244 (2000).
[28] K. Wood, S. Grudinin, B. Kessler, M. Weik, M. Johnson, G. R. Kneller, D. Oesterhelt, and G. Zaccai, J. Mol. Biol. **380**, 581 (2008).
[29] K. Nakajima, S. Ohira-Kawamura, T. Kikuchi, M. Nakamura, R. Kajimoto, Y. Inamura, N. Takahashi, K. Aizawa, K. Suzuya, K. Shibata, T. Nakatani, K. Soyama, R. Maruyama, H. Tanaka, W. Kambara, T. Iwahashi, Y. Itoh, T. Osakabe, S. Wakimoto, K. Kakurai *et al.*, J. Phys. Soc. Jpn. **80**, SB028 (2011).
[30] Y. Inamura, T. Nakatani, J. Suzuki, and T. Otomo, J. Phys. Soc. Jpn. **82**, SA031 (2013).
[31] M. Bee, *Quasielastic Neutron Scattering: Principles and Applications in Solid State Chemistry, Biology and Materials Science* (Adam Hilger, Bristol, UK, 1988).
[32] T. E. Cheatham, III, P. Cieplak, and P. A. Kollman, J. Biomol. Struct. Dyn. **16**, 845 (1999).
[33] J. Wang, P. Cieplak, and P. A. Kollman, J. Comput. Chem. **21**, 1049 (2000).

[34] W. L. Jorgensen, J. Chandrasekhar, J. D. Madura, R. W. Impey, and M. L. Klein, J. Chem. Phys. **79**, 926 (1983).
[35] D. A. Case, T. A. Darden, T. E. Cheatham, III, C. L. Simmerling, J. Wang, R. E. Duke, R. Luo, K. M. Merz, B. Wang, D. A. Pearlman, M. Crowley, S. Brozell, V. Tsui, H. Gohlke, J. Mongan, V. Hornak, G. Cui, P. Beroza, C. Schafmeister, J. W. Caldwell *et al.*, AMBER 8, University of California, San Francisco, 2004.
[36] H. J. C. Berendsen, J. P. M. Postma, W. F. van Gunsteren, A. DiNola, and J. R. Haak, J. Chem. Phys. **81**, 3684 (1984).
[37] J.-P. Ryckaert, G. Ciccotti, and H. J. C. Berendsen, J. Comput. Phys. **23**, 327 (1977).
[38] T. Darden, D. York, and L. Pedersen, J. Chem. Phys. **98**, 10089 (1993).
[39] A. Luzar and D. Chandler, Phys. Rev. Lett. **76**, 928 (1996).
[40] P. Auffinger and E. Westhof, J. Mol. Biol. **300**, 1113 (2000).
[41] W. Doster, Eur. Biophys. J. **37**, 591 (2008).
[42] F. Volino and A. J. Dianoux, Mol. Phys. **41**, 271 (1980).
[43] A. Luise, M. Falconi, and A. Desideri, Proteins **39**, 56 (2000).
[44] V. A. Makarov, B. K. Andrews, P. E. Smith, and B. M. Pettitt, Biophys. J. **79**, 2966 (2000).
[45] F. Sterpone, G. Stirnemann, and D. Laage, J. Am. Chem. Soc. **134**, 4116 (2012).
[46] M. Weik, R. B. G. Ravelli, I. Silman, J. L. Sussman, P. Gros, and J. Kroon, Protein Sci. **10**, 1953 (2001).
[47] G. Schiró, C. Caronna, F. Natali, and A. Cupane, Phys. Chem. Chem. Phys. **12**, 10215 (2010).
[48] E. Mamontov, H. O'Neill, and Q. Zhang, J. Biol. Phys. **36**, 291 (2010).
[49] M. Tarek, G. J. Martyna, and D. J. Tobias, J. Am. Chem. Soc. **122**, 10450 (2000).
[50] J. A. Hayward and J. C. Smith, Biophys. J. **82**, 1216 (2002).
[51] A. Pérez, I. Marchán, D. Svozil, J. Sponer, T. E. Cheatham, III, C. A. Laughton, and M. Orozco, Biophys. J. **92**, 3817 (2007).
[52] M. W. Mahoney and W. L. Jorgensen, J. Chem. Phys. **112**, 8910 (2000).
[53] H. W. Horn, W. C. Swope, J. W. Pitera, J. D. Madura, T. J. Dick, G. L. Hura, and T. Head-Gordon, J. Chem. Phys. **120**, 9665 (2004).
[54] I. S. Joung and T. E. Cheatham, III, J. Phys. Chem. B **112**, 9020 (2008).
[55] C. Vega, E. Sanz, and J. L. F. Abascal, J. Chem. Phys. **122**, 114507 (2005).
[56] L. Hernández de la Peña and P. G. Kusalik, J. Chem. Phys. **121**, 5992 (2004).
[57] F. J. Bermejo, K. Kinugawa, J. Dawidowski, C. Cabrillo, and R. Fernández-Perea, Chem. Phys. **317**, 198 (2005).